Supplementary Information for

Biotic induction and microbial ecological dynamics of Oceanic Anoxic Event 2

Gregory T. Connock[1]*, Jeremy D. Owens[2], Xiao-Lei Liu[1]

[1]School of Geosciences, University of Oklahoma, Norman, Oklahoma 73019, USA.

[2]Department of Earth, Ocean, and Atmospheric Science, Florida State University, and National High Magnetic Field Laboratory, Tallahassee, Florida 32306, USA.

*Corresponding author: Gregory T. Connock

Email: gtconnock@gmail.com

This PDF file includes:

Supplementary text
Figures S1 to S10
Table S1
SI References

Supplementary Discussion

Site description and novelty

Ocean Drilling Program (ODP) Leg 207 recovered mid-Cretaceous (Albian) to mid-Paleogene (Lutetian) strata from 5 sites (1257-1261) on the Demerara Rise, a gently dipping (1.5^{o}) submarine plateau ~380km north of Suriname[1] (Fig. S1). At present, the Demerara Rise is submerged ~700 mbsl, but the northwestern edge where Site 1258 was drilled (3192 mbsl) transitions to a ramp reaching depths of nearly 4000 mbsl. The Site 1258 cores capture the entirety of OAE-2 (~426-422 mcd), delineated by carbon isotope stratigraphy[2], and are predominantly composed of laminated black shales deposited in the equatorial proto-North Atlantic at intermediate water depths (500-1500m). Organic matter is abundant, thermally immature, and marine in origin within the Cenomanian-Turonian interval[1, 3-4]. Pervasive deposition of laminated black shales is not exclusive to OAE-2, signifying highly reducing bottom water conditions were a consistent feature at Site 1258[1]. A constant redox state favoring organic matter preservation is rarely observed in coeval localities, providing an advantageous framework for geochemical interpretation.

The molecular fossil record is presumed to primarily reflect a microbial signal given the locally anoxic to euxinic conditions that enveloped OAE-2. Relatively invariant carbonate-corrected total organic carbon (TOC) values prior to, during, and after OAE-2[5] (Fig. S5) highlight consistent production and/or preservation of organic matter. Black shale deposition at other localities (e.g. Furlo, Italy) is restricted to solely the OAE due to a combination of site-specific bottom water redox and sedimentation rates. Contrasting redox states preceding OAE-2 at these sites may compromise the integrity of the microbial signal, underlining the novelty of the exceptional biomarker preservation observed at the Demerara Rise[6]. Therefore, the biotic response to dynamic oceanographic conditions preceding OAE-2 is likely not ubiquitously encoded in the sedimentary archive, with the Demerara Rise an extraordinary resource for OAE research. As a result, our interpretations are not intended to be global in extent due to locality-induced preservation biases, but rather global in effect.

Furthermore, concern for post-depositional alteration of the indigenous biomarker signal is relatively low at the Demerara Rise. While subsurface microbial communities[7] do contribute lipids to the total sedimentary/fossil pool of organic compounds[8], the amount is miniscule considering their low cell abundance and long turnover time[9]. Only at specific environments with extremely high benthic microbial activity, such as methane seeps, post-depositional contribution can be sufficient to offset the original deposition signal[10]. Additional screening for biomarker precursors from living organisms (i.e. intact polar lipids) in the Demerara Rise samples yielded no detectable signal, minimizing risk of post-depositional contamination from any deep biosphere activity.

Potential source(s) of deep (bathypelagic to benthic) biomarkers

Extended archaeols, DAGEs, and BDGT/PDGT were presumed to primarily originate from microbial life residing in bathypelagic to benthic habitats. This assumption, while less certain than attribution of other biomarkers to specific organisms (e.g. isorenieratane → sulfur-oxidizing bacteria[11]), is based on multiple recent investigations substantiating the connection between these lipids and specific organisms residing at depth or in marine sediments.

The C_{25} extended archaeol is posited to modulate cell membrane dynamics by increasing membrane stability in the presence of adverse environmental conditions[12]. The extended archaeols with C_{30}, C_{35}, and C_{40} isoprenoid chains, first reported in this study, are presumed to serve a similar role as the C_{25} variant given the proposed zipper-like function of these lipids is dependent on the asymmetry of isoprenoid chain lengths[13]. This functionality is consistent with molecular surveys revealing a preponderance of C_{25} extended archaeol in Haloarchaea[14-16], leading to general acceptance that the occurrence of extended archaeol is a diagnostic biomarker for halophilic archaea and, by extension, elevated salinities[17]. Extended archaeols are classified as 'deep' biomarkers in this paper primarily due to density contrasts predisposing elevated salinities to greater depths beneath relatively less dense saline waters, which has been previously documented at the Demerara Rise[18]. Although it is possible extended archaeols may have originated from halophilic archaea beyond the bathypelagic realm if elevated salinities

shoaled, utilization of these compounds as indicators of elevated salinities is relatively unaffected by the residence depth of halophilic archaea.

The DAGEs have been increasingly linked with sulfate reducing bacteria, which predominantly reside under persistently anaerobic conditions in marine sediments[19,20]. While alternative bacterial sources exist, such as the Planctomycetes[21], sulfate-reducing bacteria represent the predominant and most likely source of these lipids. Consequently, the DAGEs are likely benthic in origin. Furthermore, DAGEs are highly resistant to diagenetic processes[22], reducing concern of post-depositional alteration to the original distribution and abundance of DAGEs in ancient sediments.

Both BDGT and PDGT, summed and referred to at BDGT/PDGT in this study, are relatively recent additions to the biomarker toolbox[23]. Initial work linked these compounds with methanogens[24], later refined to include potential contribution from heterotrophic archaea[25]. Application of BDGT/PDGT to understand depositional processes during deposition was limited in this study due to formerly mentioned uncertainties, but tentative integration with other biomarkers at the Demerara Rise revealed some paleoenvironmental potential. Despite unconstrained origins, it is likely both BDGT and PDGT were produced by benthic archaea based on intact polar lipid profiles in modern settings[25,26].

Principal component analysis

Principal component analysis (PCA) was performed on the entire dataset using RStudio Desktop (available at https://rstudio.com), an integrated development environment for R (R Core Team 2020, available at https://www.R-project.org/). Data exploration and interpretative validation were the primary motives to conduct PCA on our biomarker inventory. The prcomp() function was favored given the greater numerical accuracy of singular value decomposition compared to spectral decomposition, called by the princomp() function. Data were centered and scaled in the prcomp() function. Biplot visualization (Fig. S3) was achieved by modification of the plot() function following publicly available online guides.

Estimating the duration of the pre-OAE BP

The event duration of ~100 kyr was estimated based on the onset of the productivity spike (427.54 mcd), nearly synchronous with a minor positive $\delta^{13}C_{org}$ excursion[2] (0.83 ‰ at 427.49 mcd, Fig. S5) observed until tetrapyrrole concentrations return to pre-perturbation values at 426.88 mcd (Fig. 4). Given the notion globally enhanced carbon burial, primarily driven by elevated productivity, initiated the +CIE of OAE-2 and was perpetuated by enhanced preservation during OAE-2, we attribute the smaller positive $\delta^{13}C_{org}$ excursion to the pre-OAE BP and leverage the higher resolution $\delta^{13}C_{org}$ record to constrain pre-OAE BP duration.

Evidence for LIP trigger of the pre-OAE biotic perturbation

A spike in bioessential trace metals[5,27] (e.g. V, Mo) immediately precedes (427.63 mcd) the biotic perturbation at 427.54 mcd, where trace metals are in relatively low abundance (Fig. S4; Supplementary Data 2). This, combined with the relative timing of LIP activity[28] and continental arc volcanism[29] suggests exogenous nutrient delivery as a possible trigger for the pre-OAE BP. In addition, an abrupt increase in TEX^{H}_{86} equating to a ~1°C sea surface temperature rise coincides with the pre-OAE event (Fig. S5; Supplementary Data 3), underlining the possible role LIP-sourced and/or volcanogenic greenhouse gases played in stimulating continental erosion and runoff enriched in nutrients (e.g. PO_4^{3-}). Continental derivation of nutrients, at least at the onset, is further validated by a spike in the BIT index (branched/isoprenoid tetraether), indicative of terrestrial organic matter input[30], coeval with the precipitate trace metal incursion. Consistency between trace metal and BIT index behavior throughout the pre-OAE biotic shift (427.54-426.40 mcd, Fig. S4-5, 8) implies similar controlling processes, something unobserved during OAE-2. The departure from trace metal (e.g. V) and BIT index covariance during OAE-2 (Fig. S8) is likely a result of increased production of aquatic brGDGTs in an expanded OMZ, which adversely affected crenarchaeol production by *Thaumarchaeota*. Relative increases in 6-methyl penta- and hexamethylated brGDGTs to 5-methyl penta- and hexamethylated brGDGTs, previously used to differentiate soil vs. aquatic brGDGT synthesis[31], coincided with elevated BIT values and provide evidence for multiple controls on brGDGT distributions (Fig. S8; Supplementary Data 3). This

results in an increase in the numerator (brGDGTs) and decrease in the denominator (crenarchaeol) of the BIT index, explaining the elevated BIT indices observed during OAE-2. Regarding the pre-OAE trigger mechanism(s), either fluvial discharge was the primary source of trace metals or was coincidental with ocean fertilization by LIP-related hydrothermal fluids rich in trace metals. Nevertheless, one or both processes provided an injection of nutrients [partially] culpable for initiating the pre-OAE biotic perturbation.

Tetrapyrroles as a record of primary production

It is critical to provide a complete discussion outlining our rationale to employ the tetrapyrroles (free base chlorins, porphyrins and metalloporphyrins) as a record of productivity in the Cenomanian-Turonian equatorial North Atlantic Ocean. Tetrapyrrole investigations are disconnected in time, as initial popularity of these fossil chlorophylls diminished until relatively recent pursuits targeted reconstruction of ancient N cycling dynamics. A previous study of free base and metallo (VO, Zn) C_{33} bicycloalkanoporphyrins (BiCAPs) at Site 1261 of the Demerara Rise concluded tetrapyrrole stratigraphic abundance was primarily a function of metal accessibility, and not bottom water redox or maturity[32]. We agree maturity and redox state exerted a minimal effect on tetrapyrrole preservation. The narrow stratigraphic window of the studied section (~10 m) ensures comparable levels of thermal stress imparted a consistent, albeit negligible, influence on tetrapyrrole distribution. Similarly, the exceptional preservation present at the Demerara Rise before, during, and after OAE-2 limits preservation biases. However, a shift to euxinic conditions likely impacted the availability of metals reactive with sulfides[33] (e.g. Ni), which will in turn affect relevant metalloporphyrin formation. Other metals (e.g. V) will complex with organic matter under reducing conditions[34], competing with porphyrin chelation. Although expanded euxinia and enhanced organic matter preservation typify OAE-2, characterized by relatively low concentrations of trace metals, free base chlorins, porphyrins, and metalloporphyrins, our observations suggest relative changes in chlorophyll production (i.e. primary production) exerted greater control on tetrapyrrole abundance at the Demerara Rise.

Overall, high tetrapyrrole concentrations are not exclusively linked to high metal concentrations. The free base chlorins and porphyrins should not be sensitive to metal availability and display no significant relationship with V (Fig. S9), Zn, Mo, or Fe. Identified metalloporphyrins (VO, Ni, Zn, Fe) also exhibit a weak correlation to formerly mentioned metals. High metalloporphyrin concentrations are observed at relatively low and high metal abundances (Supplementary Data 2). If a group of samples, partially comprised of data from the pre-OAE biotic perturbation, with high metalloporphyrin concentrations relative to depressed trace metal (e.g. V) values is removed, then a strong positive relationship emerges (Fig. S9). This suggests metal availability does play a role in metalloporphyrin abundance, but to what extent remains unconstrained as other processes (e.g. supply of free base porphyrins) may also impact the absolute metalloporphyrin concentrations. Despite the ambiguity surrounding the impact of metal availability on tetrapyrrole preservation, it is clear the presence of metals, particularly V, facilitates the metalation of free bases. A strong negative linear relationship was observed between the ratio of free bases to metalloporphyrins and V (R^2 = 0.86; Fig. S9). Therefore, metal abundance plays a key role in metalloporphyrin formation if sufficient precursor is available but does not influence the absolute concentration of porphyrins in sediments.

On average, free base tetrapyrroles (chlorins + porphyrins) are an order of magnitude greater in concentration relative to metalloporphyrins in our study (Fig. 4, Data S2). Given free base tetrapyrroles lack any significant relationship to metal supply and the Cenomanian-Turonian at Site 1258 was deposited under relatively constant reducing conditions, the total tetrapyrrole profile (free base + metallo; Fig. 4) is primarily indicative of chlorophyll production and reflective of relative variations in primary production. Inclusion of the metalloporphyrins, which mostly mirror the free base tetrapyrroles over the analyzed section (Fig. 4, S4), helps diminish diagenetic alteration of the primary producer signal. However, uncharacterized complexity influencing metalloporphyrin distributions precludes application in isolation of free base tetrapyrroles. For example, the metalloporphyrins were present in greatest concentrations prior to OAE-2 and do not recover to comparable levels post-OAE as trace metals and free base tetrapyrroles rebound (Fig. 4, S4). It is beyond the scope of this study to elucidate additional controls on

metalloporphyrin formation, but the progressive alteration of the original chlorophyll risks deterioration of the original primary producer signal.

LC-qTOF-MS method reproducibility and detection limits

Triplicates were run for three exemplary samples from the pre-OAE, OAE, and post-OAE intervals to determine reproducibility of the modified LC-qTOF-MS method used in this study. All samples were subjected to identical instrumental conditions following procedures outlined in the methods section. Representative biomarkers from each analyzed compound suite were selected for integration and quantification relative to an internal standard as previously described. Coefficient of variation (i.e. relative standard deviation) was calculated for each biomarker, ranging from 1% to 3.7% (Table S1), which underscores the high reproducibility of our modified LC-qTOF-MS method.

Detection limits were established by comparing signal intensity of the internal standard to the background noise of the sample. Injection of a C_{46} GTGT standard solution revealed exceedingly low on-column detection limits less than 0.001 ng with a signal intensity of approximately $1.5 * 10^3$ (Fig. S10). However, when the standard solution was used to spike a sediment extract for biomarker quantification, on-column detection limits were slightly greater than 0.001 ng due to background signal intensities of ~$1.0 * 10^3$ (Fig. S10). Most biomarkers were well above the detection limit established here, and are reported as not detected (n.d.) when these limits were exceeded. For example, the extracted aliquot of sample 1258B 45-R4 148-149 contained ~44,000 ng_{cren} g^{-1} OC and had an organic carbon content of 0.0185 g. Post-drying, 1 mL of MeOH was added to all samples and 10 µL was injected on-column, resulting in ~8 ng of crenarchaeol to be introduced directly onto the column, several orders of magnitude greater than detection limits. Thus, the applied LC-qTOF-MS method exhibited the necessary reproducibility and sensitivity to accurately measure and quantify biomarker concentrations across OAE-2 at the Demerara Rise in this study.

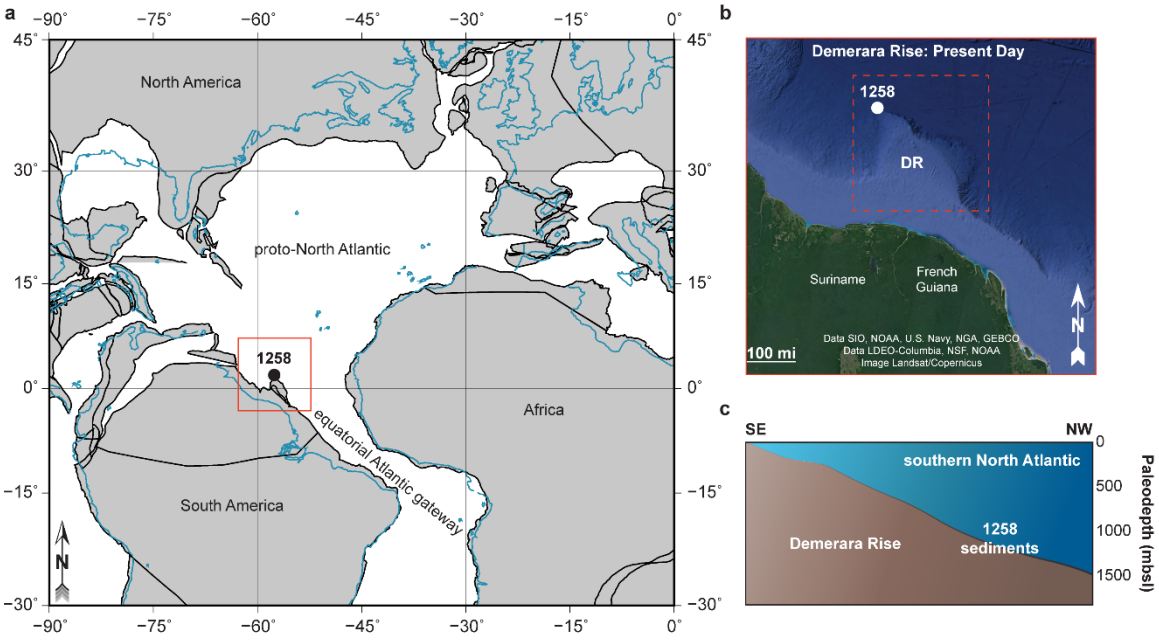

Fig. S1. Paleogeographic location and depositional setting of the Demerara Rise. (A) Paleogeographic position of the Demerara Rise in the southern proto-North Atlantic at ~93.9Ma. Gray shaded regions bounded by black lines represent continental plates and blue signifies present day shorelines (GEOMAR map generator; https://www.odsn.de/odsn/services/paleomap/paleomap.html). The red box and labeled black circle highlight the study area. **(B)** Present day satellite imagery of the Demerara Rise, with the study area labeled by a white circle (imagery data compiled and retrieved from Google Earth, data: SIO, NOAA, U.S. Navy, NGA, GEBCO, LDEO-Columbia, NSF, NOAA, image: Landsat/Copernicus). **(C)** Illustration depicting the relative paleodepth (meters below sea level) of 1258 sediment deposition at ~93.9Ma.

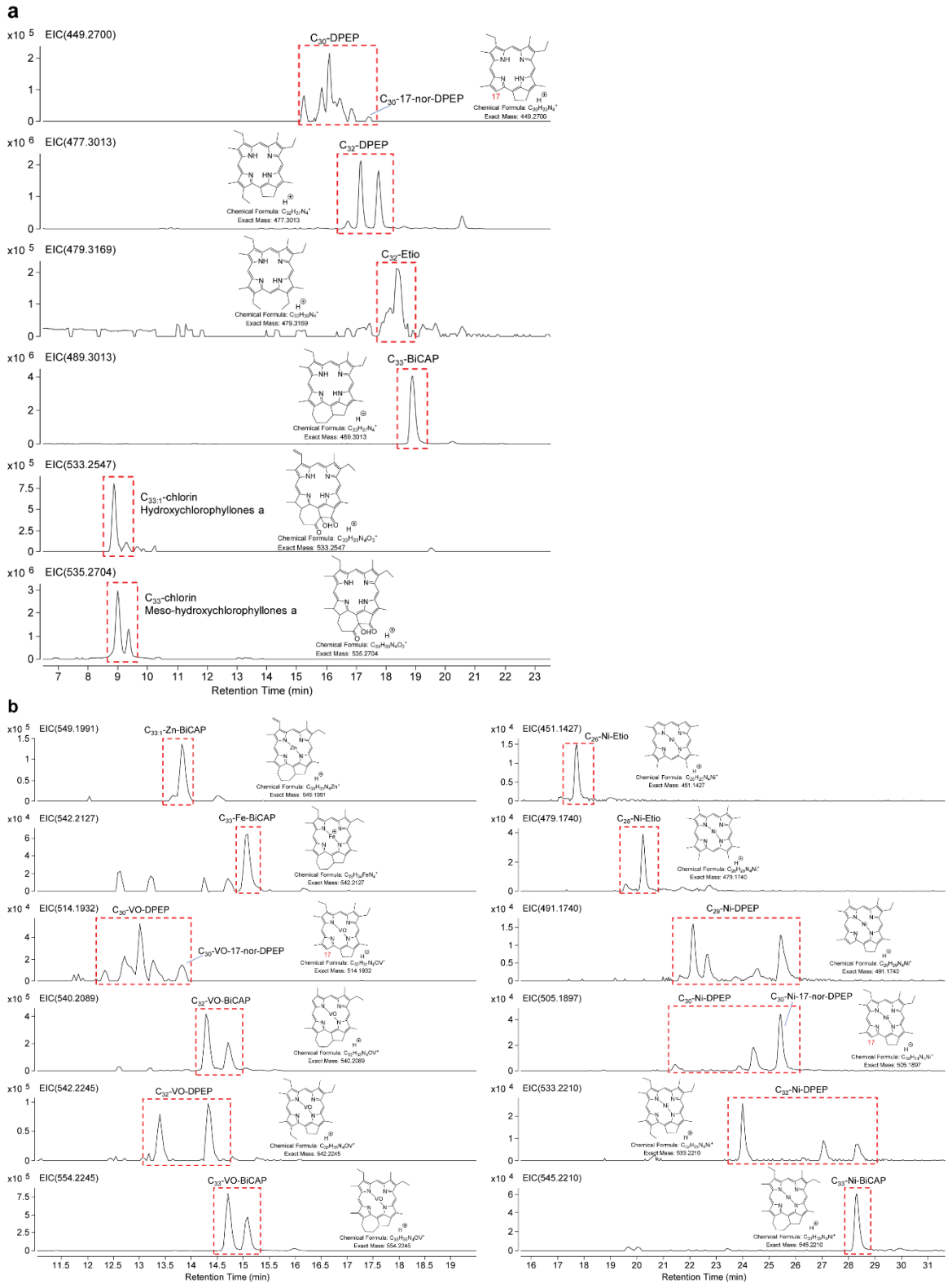
a
EIC(449.2700)
C30-DPEP
C30-17-nor-DPEP
EIC(477.3013)
C32-DPEP
EIC(479.3169)
C32-Etio
EIC(489.3013)
C33-BiCAP
EIC(533.2547)
C33:1-chlorin
Hydroxychlorophyllones a
EIC(535.2704)
C33-chlorin
Meso-hydroxychlorophyllones a
Retention Time (min)
b
EIC(549.1991)
C33:1-Zn-BiCAP
EIC(542.2127)
C33-Fe-BiCAP
EIC(514.1932)
C30-VO-DPEP
C30-VO-17-nor-DPEP
EIC(540.2089)
C32-VO-BiCAP
EIC(542.2245)
C32-VO-DPEP
EIC(554.2245)
C33-VO-BiCAP
EIC(451.1427)
C26-Ni-Etio
EIC(479.1740)
C28-Ni-Etio
EIC(491.1740)
C28-Ni-DPEP
EIC(505.1897)
C30-Ni-DPEP
C30-Ni-17-nor-DPEP
EIC(533.2210)
C32-Ni-DPEP
EIC(545.2210)
C33-Ni-BiCAP
Retention Time (min)

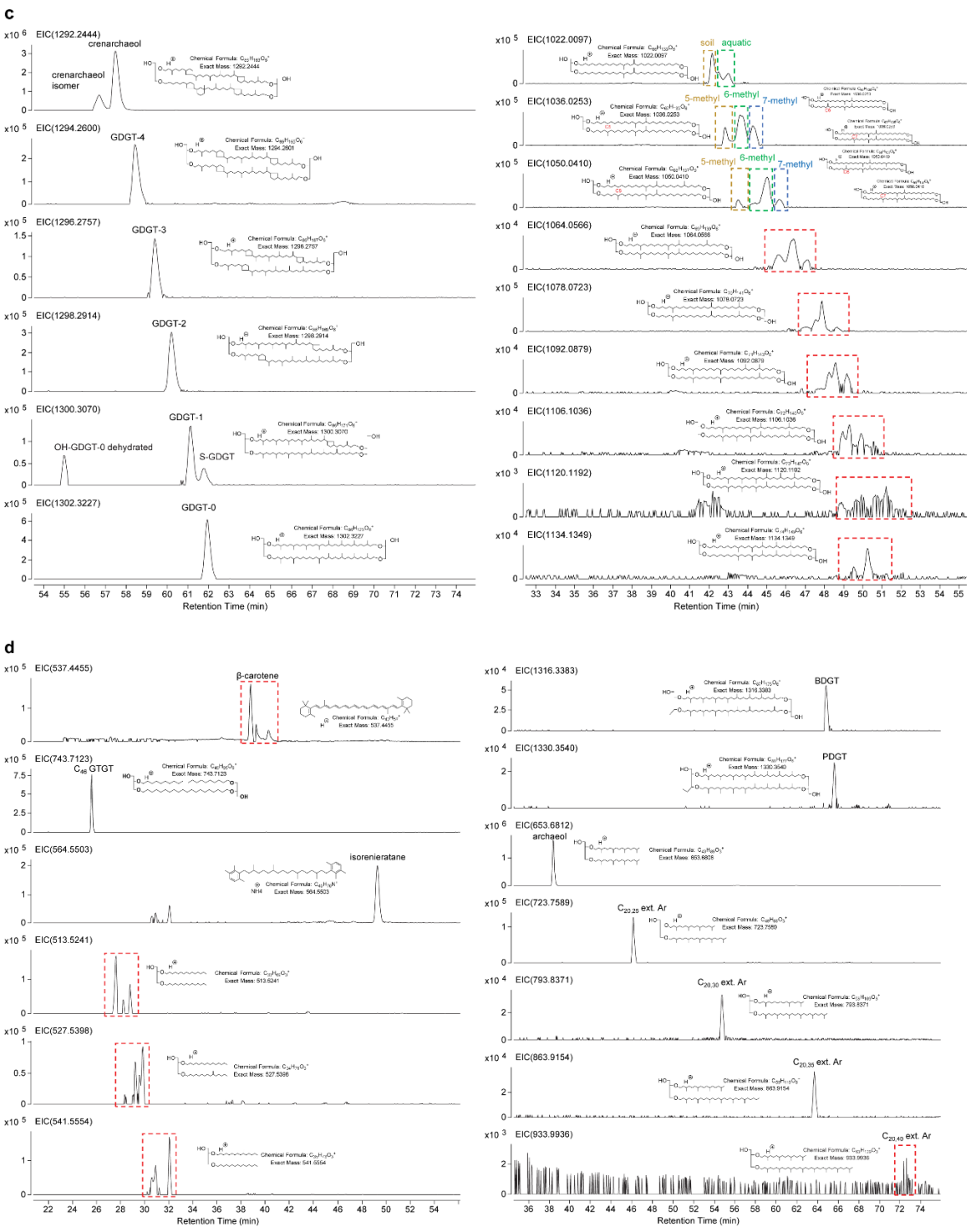

Fig. S2. Extracted ion chromatograms (EICs) of identified biomarkers. (a) Free base porphyrins and chlorins detected in sample 1258A 42-6 82-83. **(b)** Major VO-, Zn-, Fe- and Ni-porphyrins detected in sample 1258A_42-6 17-18. **(c)** isoGDGTs, brGDGTs and obGDGTs detected in sample 1258A 42-6 82-83. **(d)** Internal standards (β-carotene and C_{46} GTGT), isorenieratane, DAGEs, BDGT, PDGT, archaeol, and extended archaeols shown in sample 1258A 42-6 82-83.

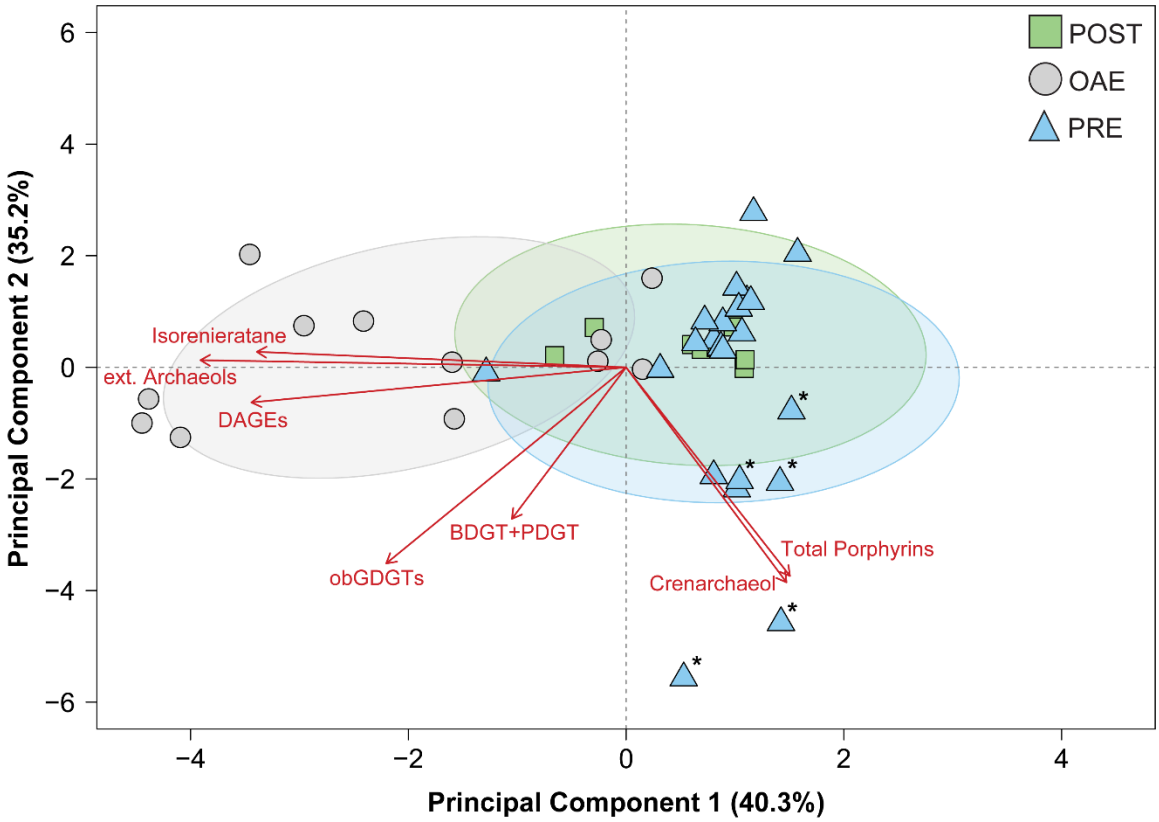

Fig. S3. PCA results of biomarkers utilized in this study. Note the separation, driven primarily by biomarkers sourced from intermediate and deep waters, of pre- and post-OAE strata from samples deposited during the OAE. Samples with a '*' are from the pre-OAE biotic perturbation.

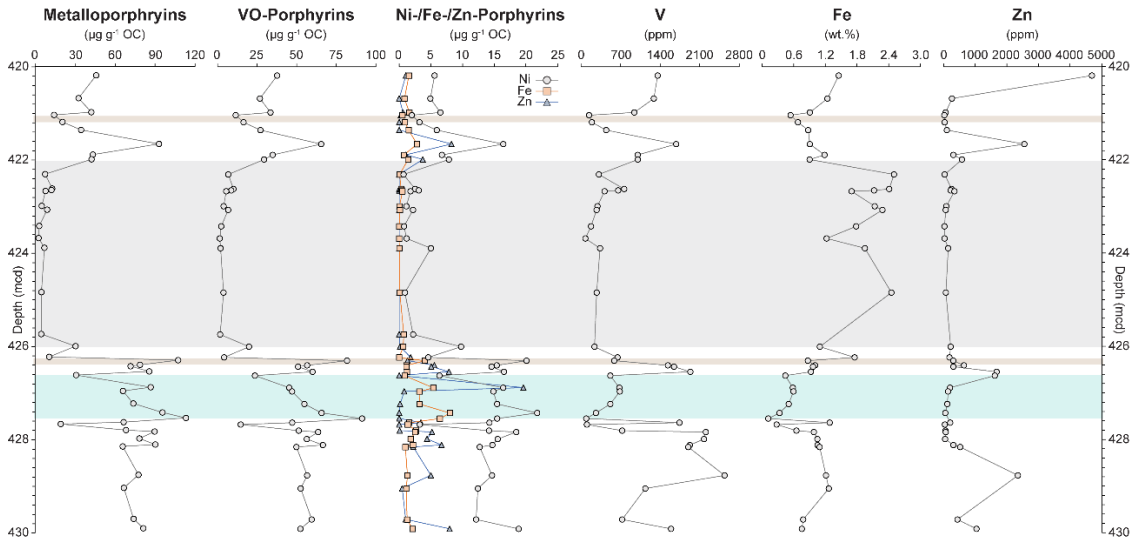

Fig. S4. Depth profiles of metalloporphyrins and trace metals through the studied section. All metalloporphyrin data were generated in this study, with trace metal data from previous work[5,27]. The blue shaded interval represents the pre-OAE biotic perturbation, the gray shaded interval represents OAE-2, and the brown shaded intervals represent the positive Tl isotopic excursions.

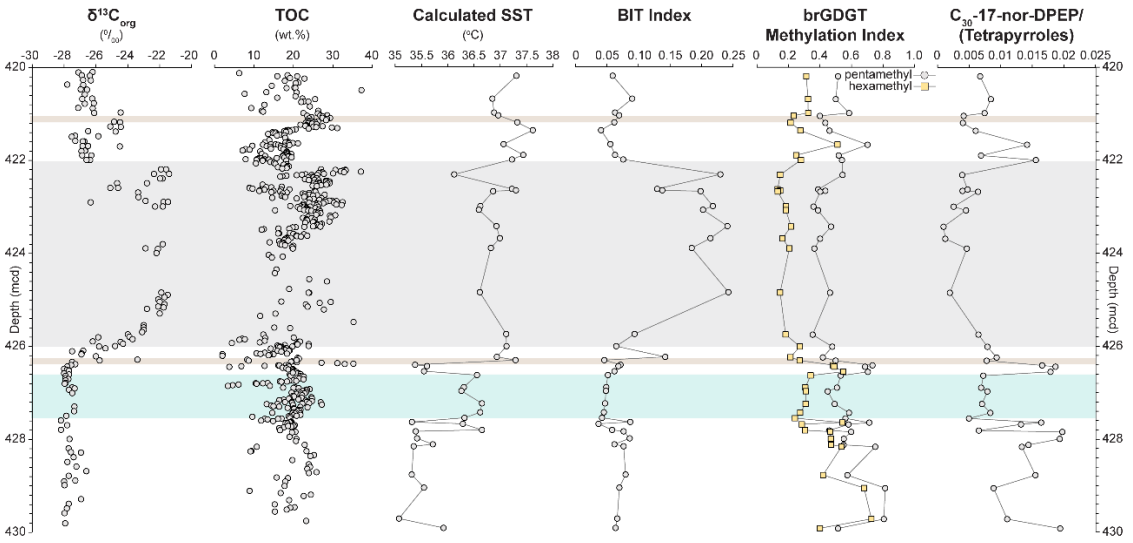

Fig. S5. Various geochemical profiles from Site 1258, Demerara Rise. The $\delta^{13}C_{org}$ and TOC values are compiled from previous studies[2,5,27]. Sea surface temperatures (SST) were calculated from TEX^{H}_{86} using published methods[35,36]. Similarly, BIT indices were calculated based on previously published work[30]. The brGDGT methylation index is simply the ratio of the 5-methyl normalized to the 6-methyl penta-/hexa-methyl brGDGTs, similar to prior reports[31]. The C_{30}-17-nor-DPEP is normalized to the total summed tetrapyrroles, including free base chlorins, porphyrins, and metalloporphyrins. The blue shaded interval represents the pre-OAE biotic perturbation, the gray shaded interval represents OAE-2, and the brown shaded intervals represent the positive Tl isotopic excursions.

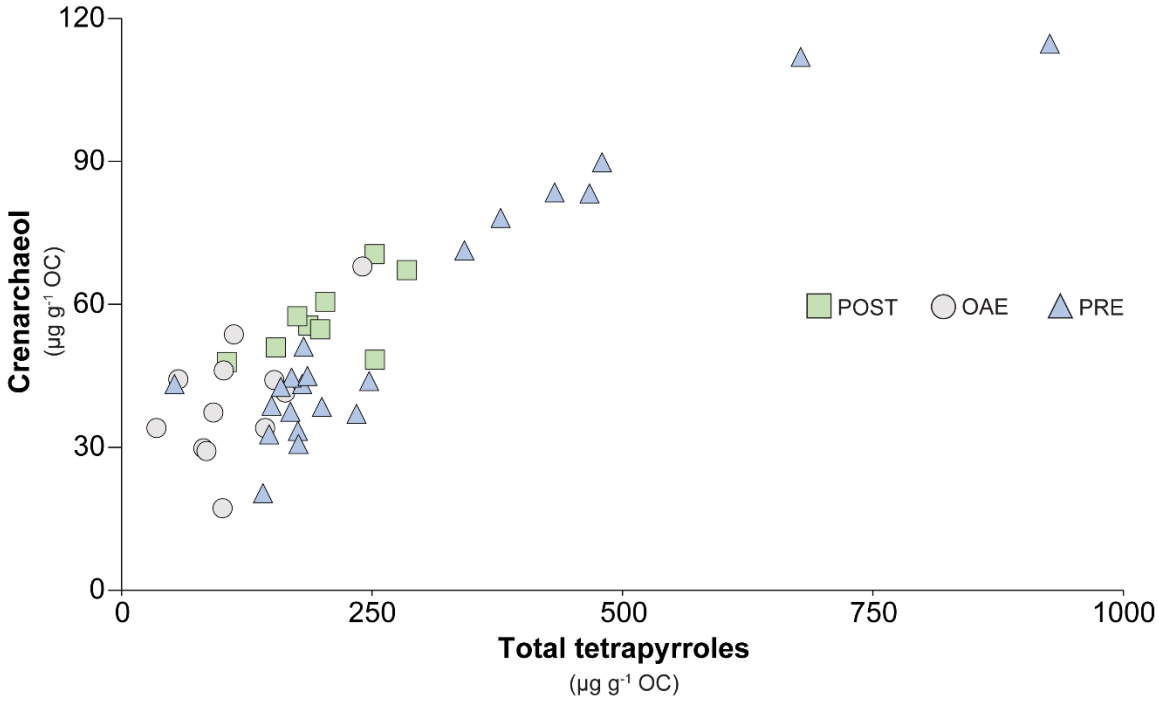

Fig. S6. Cross plot of crenarchaeol and summed tetrapyrrole (chlorins, free base porphyrins, and metalloporphyrins) concentrations.

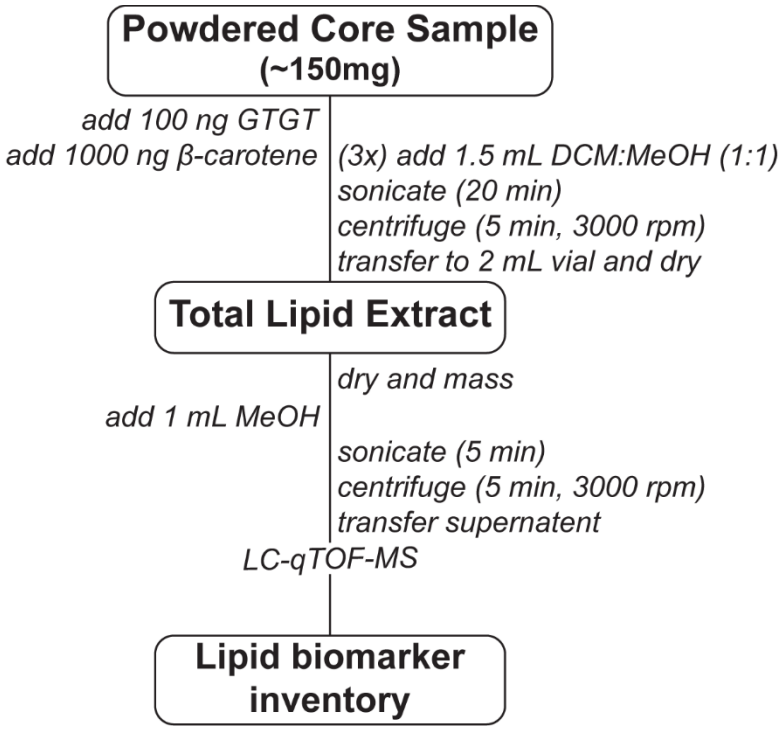

Fig. S7. Preparatory procedure for extraction and analysis of biomarkers.

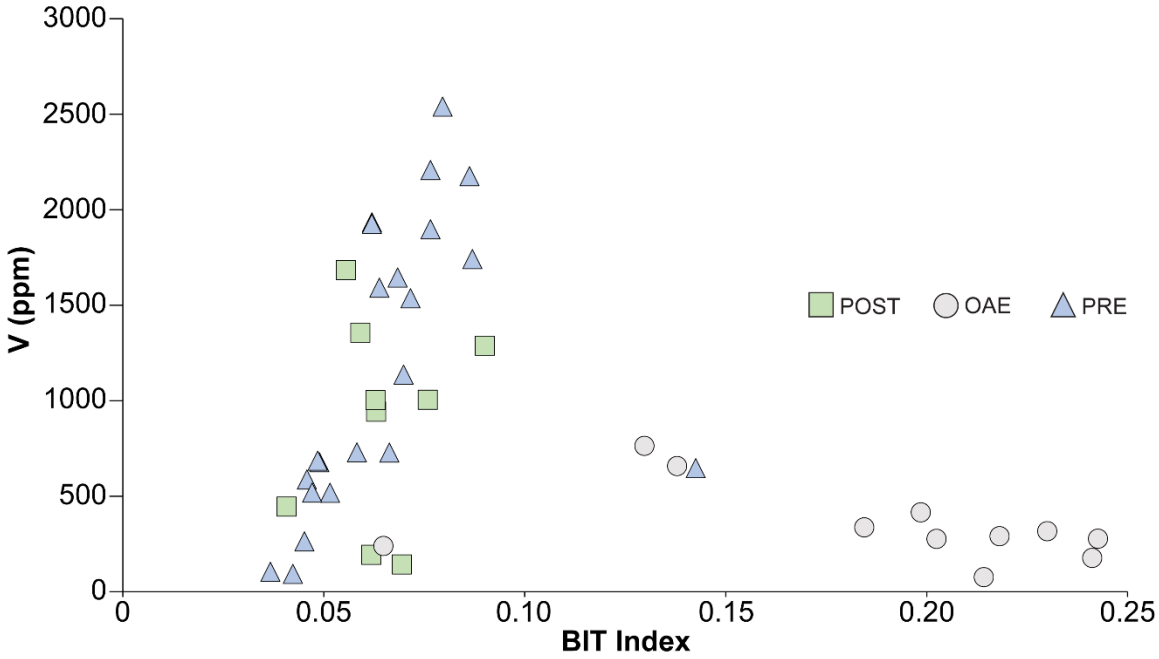

Fig. S8. Cross plot of V and BIT Index. Note the duality of the relationship between BIT indices and V concentrations. Pre- and post-OAE strata predominantly exhibited a positive relationship between trace metal abundance and BIT indices, whereas most OAE-2 samples displayed a negative correlation between the two variables.

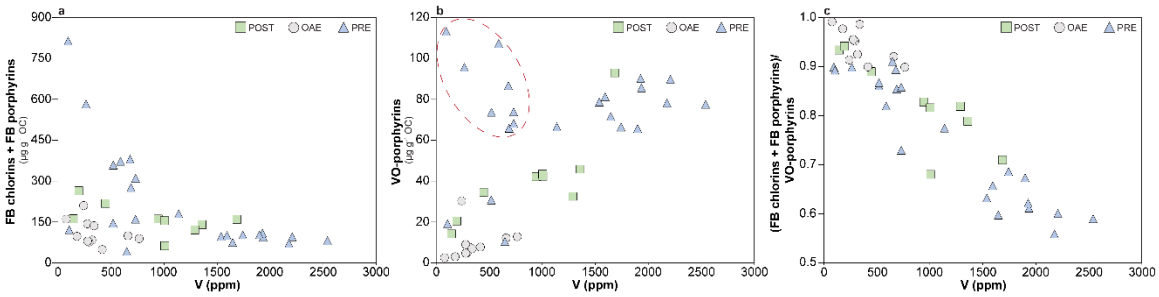

Fig. S9. Cross plots of various tetrapyrroles and V. (**a**) Cross plot of the free base chlorins and porphyrins with V. (b) Cross plot of the VO-metalloporphyrins and V. Note the cluster of pre-OAE samples, encircled by the red hashed outline, exhibiting relatively high metalloporphyrin content for a given range of V concentrations. Otherwise, a clear positive correlation would exist between metalloporphyrins and V. (**c**) The ratio of free base chlorins and porphyrins to metalloporphyrins against V levels.

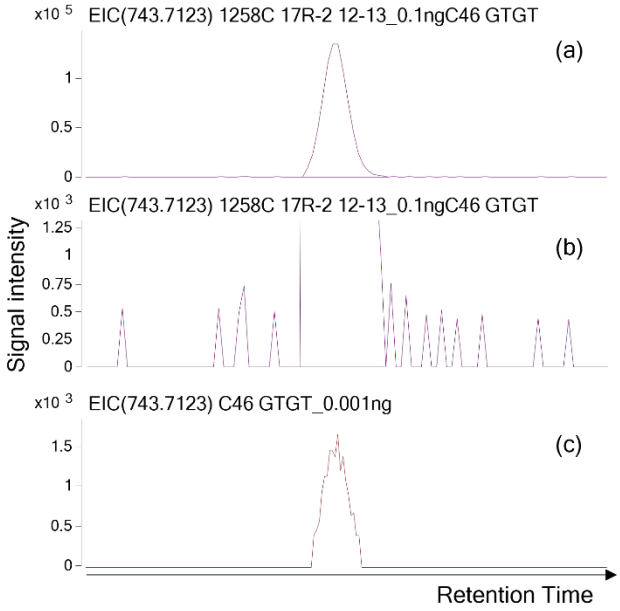

Fig. S10. Extracted ion chromatograms (EICs) of the internal standard, C_{46} GTGT, in standard solution (c) and a sample from the Demerara Rise (a-b) generated by the modified LC-qTOF-MS method. Sample 1258C 17R-2 12-13 was spiked with C_{46} GTGT, resulting in ~0.1ng of C_{46} GTGT to be injected on-column, with EICs of the extract (a) and background noise (b). Reliable detections require analyte signal intensities to exceed background noise. Compared signal intensity of 0.1ng of C46 GTGT standard (~1.5 * 10^5) and background noise (~1 * 10^3) of an analyzed sediment extract, 1258C 17R-2 12-13, and 0.001ng C_{46} GTGT (~1.5 * 10^3) in standard solution indicate a detection limit of C_{46} GTGT in sediment extracts, and by extension targeted biomarkers, that is slightly greater than 0.001ng on-column.

Samples	C_{33}-chlorin	Crenarchaeol	Isorenieratane	C_{70}-obGDGT	C_{33}-DAGE	Archaeol
1258A 42-5 51-53_1	3.681	29.735	0.025	0.656	0.180	4.242
1258A 42-5 51-53_2	3.717	30.923	0.026	0.683	0.179	4.345
1258A 42-5 51-53_3	3.894	32.025	0.026	0.704	0.170	4.529
Average	*3.764*	*30.894*	*0.026*	*0.681*	*0.176*	*4.372*
Standard Deviation	*0.114*	*1.145*	*0.001*	*0.024*	*0.006*	*0.145*
Coefficient of Variation	***0.030***	***0.037***	***0.019***	***0.036***	***0.033***	***0.033***
1258B 45R-4 148-149_1	6.345	13.954	0.490	0.768	0.570	7.971
1258B 45R-4 148-149_2	6.480	14.254	0.473	0.790	0.571	8.160
1258B 45R-4 148-149_3	6.542	13.999	0.504	0.769	0.580	8.087
Average	*6.455*	*14.069*	*0.489*	*0.776*	*0.574*	*8.073*
Standard Deviation	*0.101*	*0.162*	*0.015*	*0.012*	*0.006*	*0.095*
Coefficient of Variation	***0.016***	***0.012***	***0.032***	***0.015***	***0.010***	***0.012***
1258C 17R-2 12-13_1	0.390	14.166	0.031	0.459	0.078	3.276
1258C 17R-2 12-13_2	0.384	13.804	0.029	0.448	0.074	3.244
1258C 17R-2 12-13_3	0.375	13.766	0.029	0.430	0.074	3.203
Average	*0.383*	*13.912*	*0.029*	*0.446*	*0.075*	*3.241*
Standard Deviation	*0.008*	*0.221*	*0.001*	*0.015*	*0.002*	*0.036*
Coefficient of Variation	***0.020***	***0.016***	***0.035***	***0.034***	***0.031***	***0.011***

Table S1. Calculated values of coefficient of variation (<0.04) determined from triplicate injections of three representative samples. Multiple runs of 1258A 42-5 51-53 (post-OAE), 1258B 45R-4 148-149 (OAE-2), and 1258C 17R-2 12-13 (pre-OAE) confirm reproducibility of our applied quantitative LC-qTOF-MS analyses. β-carotene was used as internal standard for the quantification of isorenieratane, and C_{46} GTGT for the other compounds. Column values represent the on-column abundances of each biomarker in ng.

SI References

1. J. Erbacher, D. C. Mosher, M. J. Malone, *Proc. ODP Init. Rep.* 207 (2004).
2. J. Erbacher, O. Friedrich, P. A. Wilson, H. Birch, J. Mutterlose, Stable organic carbon isotope stratigraphy across Oceanic Anoxic Event 2 of Demerara Rise, western tropical Atlantic. *Geochem. Geophys. Geosyst*. **6**, Q06010 (2005).
3. A. Forster, H. Sturt, P. A. Meyers, *Proc. ODP Init. Rep.* 207 (2004).
4. P. A. Meyers, S. M. Bernasconi, A. Forster, Origins and accumulation of organic matter in expanded Albian to Santonian black shale sequences on the Demerara Rise, South America margin. *Org. Geochem.* **37**, 1816-1830 (2006).
5. J. D. Owens, C. T. Reinhard, M. Rohrssen, G. D. Love, T. W. Lyons, Empirical links between trace metal cycling and marine microbial ecology during a large perturbation to Earth's carbon cycle. *Earth Planet. Sci. Lett*. **449**, 407-417 (2016).
6. C. K. Junium, B. J. Keely, K. H. Freeman, M. A. Arthur, Chlorins in mid-Cretaceous black shales of the Demerara Rise: The oldest known occurrence. *Org. Geochem*. **42**, 856-859 (2011).
7. F. Inagaki *et al*. Exploring deep microbial life in coal-bearing sediment down to ~2.5 km below the ocean floor. *Science,* **349**, 420-424. (2015).
8. J. S. Lipp, Y. Morono, F. Inagaki, K.-U. Hinrichs. Significant contribution of Archaea to extant biomass in marine subsurface sediments. *Nature*, **454**, 991-994. (2008).
9. S. Xie, J. S. Lipp, G. Wegener, T. G. Ferdelman, K.-U. Hinrichs. Turnover of microbial lipids in the deep biosphere and growth of benthic archeael populations. *Proc. Natl. Acad. Sci. U.S.A.* **110**, 6010-6014 (2013).
10. X.-L. Liu, J. S. Lipp, K.-U. Hinrichs. Distribution of intact and core GDGTs in marine sediments. *Organic Geochemisty,* **42**, 368-375. (2011).
11. S. Liaaen-Jensen, Bacterial carotenoids, *Acta Chem. Scandinavica*. **19**, 1025-1030 (1965).
12. M. Y. Kellermann, M. Y. Yoshinaga, R. C. Valentine, L. Wörmer, D. L. Valentine, Important roles for membrane lipids in haloarchaeal bioenergetics. *Biochimica et Biophysica Acta*, **1858**, 2940-2956. (2016).
13. M. DeRosa et al., An asymmetric archaebacterial diether lipid from alkaliphilic halophiles. *Journal Gen. Microbiol*. **128**, 343-348 (1982).
14. N. J. Bale et al., New insights into the polar lipid composition of extremely halo(alkali)philic Euryarchaea from hypersaline lakes. *Front. Microbio*. **10**, 377 (2019).
15. K. S. Dawson, K. H. Freeman, J. L. Macalady, Molecular characterization of core lipids from halophilic archaea grown under different salinity conditions. *Organic Geochemistry*, **48**, 1-8. (2012).
16. L. Villanueva, J. S. Sinninghe Damsté, S. Schouten, A re-evaluation of the archaeal membrane lipid biosynthetic pathway. *Nat. Rev. Microbiol*., **12**, 438-448. (2014).
17. F. Vandier, M. Tourte, C. Doumbe-Kingue, J. Plancq, P. Schaeffer, Reappraisal of archaeal C_{20}-C_{25} diether lipid (extended archaeol) origin and use as a biomarker of hypersalinity. *Organic Geochemistry*, **159**, 104276. (2021).
18. A. Jiménez Berrocoso, K. G. MacLeod, E. E. Martin, E. Bourbon, C. I. Londoño, C. Basak, Nutrient trap for Late Cretaceous organic-rich black shales in the tropical North Atlantic. *Geology*, **38**, 1111-1114. (2010).
19. H. Niemann, M. Elvert, Diagnostic lipid biomarker and stable carbon isotope signatures of microbial communities mediating the anaerobic oxidation of methane with sulphate. *Organic Geochemistry,* **39**, 1668-1677. (2008).
20. A. Vinçon-Laugier, V. Grossi, M. Pacton, G. Escarguel, C. Cravo-Laureau, The alkyl glycerol ether lipid composition of heterotrophic sulfate reducing bacteria strongly depends on growth substrate. *Organic Geochemistry*, **98**, 141-154. (2016).
21. J. S. Sinninghe Damsté, W. I. C. Rijpstra, J. A. J. Geenevasen, M. Strous, M. S. M. Jetten, Structural identification of ladderane and other membrane lipids of Planctomycetes capable of anaerobic ammonium oxidation (annamox). *FEBS J.,* **272**, 4270-4283. (2005).

22. A. Vinçon-Laugier, C. Cravo-Laureau, V. Grossi, Selective preservation among bacterial alkyl glycerol ether lipid structures during long term oxic and anoxic incubation. *Organic Geochemistry*, **125**, 24-28. (2018).
23. C. Zhu, T. B. Meador, W. Dummann, K.-U. Hinrichs, Identification of unusual butanetriol dialkyl glycerol tetraether and pentanetriol dialkyl glycerol tetraether lipids in marine sediments. *Rapid Commun. Mass Sp.,* **28**, 332-338. (2014).
24. K. W. Becker, F. J. Elling, M. Y. Yoshinaga, A. Söllinger, T. Urich, K.-U. Hinrichs, Unusual butane- and pentanetriol-based tetraether lipids in *Methanomassiliicoccus luminyensis*, a representative of the seventh order of methanogens. *Applied and Environmental Microbiology*, **82**, 4505-4516. (2016).
25. S. Coffinet et al., Structural elucidation and environmental distributions of butanetriol and pentanetriol dialkyl glycerol tetraethers (BDGTs and PDGTs). *Biogeosci*. **17**, 217-330 (2020).
26. T. B. Meador, M. Bowles, C. S. Lazar, C. Zhu, A. Teske, K.-U. Hinrichs, The archaeal lipidome in estuarine sediment dominated by members of the miscellaneous crenarchaeotal group. *Environmental Microbiology,* **17**, 2441-2458. (2015).
27. A. Hetzel, M. E. Böttcher, U. G. Wortmann, H.-J. Brumsack, Paleo-redox conditions during OAE 2 reflected in Demerara Rise sediment geochemistry (ODP Leg 207). *Palaeogeog, Palaeoclim, Palaeoeco.* **273**, 302-328 (2009).
28. A. D. C. Du Vivier et al., Marine 187Os/188Os isotope stratigraphy reveals the interaction of volcanism and ocean circulation during Oceanic Anoxic Event 2. *Earth Planet. Sci. Lett*. **389**, 23-33 (2014).
29. C.-T. A. Lee *et al*., Volcanic ash as a driver of enhanced organic carbon burial in the Cretaceous. *Sci. Rep.* **8:4197** (2018).
30. E. C. Hopmans *et al*., A novel proxy for terrestrial organic matter in sediments based on branched and isoprenoid tetraether lipids. *Earth Planet. Sci. Lett.* **224**, 107-116 (2004).
31. W. Xiao *et al*., Ubiquitous production of branched glycerol dialkyl glycerol tetraethers (brGDGTs) in global marine environments: a new source indicator for brGDGTs. *Biogeosci.* **13**, 5883-5894 (2016).
32. C. K. Junium, K. H. Freeman, M. A. Arthur, Controls on the stratigraphic distribution and nitrogen isotopic composition of zinc, vanadyl and free base porphyrins through Oceanic Anoxic Event 2 at Demerara Rise. *Org. Geochem*. **80**, 60-71 (2015).
33. M. D. Lewan, Factors controlling the proportionality of vanadium to nickel in crude oils. *Geochim. Cosmochim. Acta.* **48**, 2231-2238.
34. G. N. Breit, R. B. Wanty, Vanadium accumulation in carbonaceous rocks – a review of geochemical controls during deposition and diagenesis. *Chem. Geol.* **91**, 83-97 (1991).
35. S. Schouten, E. C. Hopmans, E. Schefuß, J. S. Sinninghe Damsté, Distributional variations in marine crenarchaeotal membrane lipids: A new tool for reconstructing ancient sea water temperatures*? Earth Planet. Sci. Lett.* **204**, 265-274 (2002).
36. J. H. Kim *et al*., New indices and calibrations derived from the distribution of crenarchaeal isoprenoid tetraether lipids: Implications for past sea surface temperature reconstructions. *Geochim. Cosmochim. Acta.* **74**, 4639-4654 (2010).